

ORIGINAL RESEARCH

Modelling, synthesis, fabrication, and characterization of a novel lead-free organo-inorganic iodide perovskite for photovoltaic application

Abdulkareem Bello¹, Adam U. Alhaji², Mahdi Makoyo², Nurudeen Salahudeen³, Farhana Aziz⁴, Ojo Samuel⁴

Received: 24th March, 2023 / Accepted: 10th October, 2023

Published online: 28th October, 2023

Abstract

This work is aimed at modelling, synthesizing, and characterizing of a novel lead-free organo-inorganic halide perovskite for photovoltaic application. A planar solar cell device architecture was employed in the fabrication with graphite anode. Thermogravimetry analyzer (TGA) was used to determine the thermal stability under nitrogen flow from 20 °C to 870 °C. The TGA result exhibits thermal stability above 200 °C. X-Ray Diffraction (XRD) was used to confirm the crystallinity formation, several peaks were observed with the most prominent peaks at $2\theta = 19.0^\circ$, 29.5° , and 33.3° with average crystalline size of 42 nm calculated using Scherrer's equation. The Field Emission Scan Electron Microscope/Energy Dispersion Spectroscopy (FESEM/EDS) results showed a plate-like/cubic structure of hexagonal crystal shapes. These shapes are agglomerated in nature with fine and coarse grains, which might improve the photo-excited electrons diffusion through aggregating the light scattering properties and effective mean path of light of perovskite solar cell. Differential Scanning Calorimetry (DSC) results showed that gradual decomposition of the material can only be visible between 200 °C and 240 °C with the peak at 223.9 °C. The photoluminescence properties of the synthesized perovskites light absorbing layers exhibit a broad band spectrum emission within the range of 340 to 588nm, which is within visible spectrum. The UV-vis spectrum exhibits a strong optical absorption band in the visible region, which extends from 360 nm to 725 nm. The band gap energy was calculated from the plotted Tauc fit and estimated to be 1.99 eV. The J-V of the synthesized material recorded the highest PCE of 4.6 % with a fill factor of 19.56.

Keywords: Perovskite, Tetramethylammonium Iodide, Barium Iodide, Stability, Band Gap, Glacial Acetic

Introduction

Perovskites have the empirical formula ABX_3 where, A and B are two cations of different sizes and X is an anion that bonds to both (Warner, 2012). X is originally oxygen but also other anion such as halides, sulphides and nitrides can fit in its site as shown in Figure 1.

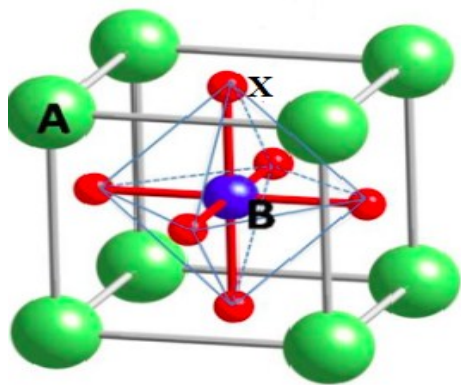


Figure 1 Crystal structure of a typical perovskite structure (Green *et al.*, 2014)

Recently, hybrid halide perovskite was discovered to possess photoelectric effect. This means that it can be used to harvest solar energy for man use. Hybrid perovskite solar cell was

introduced by Miyasaka *et al* in 2009 with a power conversion efficiency (PCE) of 3.8 %. Few years later, the PCE of PSCs has reached to 25.7 % (Ding *et al.*, 2018). This competitive increase in its efficiency has been made possible due to the unique optoelectronic properties of the hybrid perovskites (Dong *et al.*, 2015; Xing *et al.*, 2013; Stranks *et al.*, 2013; Shi *et al.*, 2015; Lian *et al.* (2016). Minemoto *et al.* (2015) such as direct band gap, high absorption coefficient, and charge transport properties. However, this remarkable improvement in the power conversion efficiency of hybrid halide perovskite is deterred by the poor air stability of perovskite absorbers. This is basically true for polycrystalline thin films perovskite solar cells because their performance is drastically affected by the shorter diffusion length and high trap state densities (Dong *et al.*, 2015; Minemoto *et al.*, 2015). In contrast, perovskite single crystals exhibit low trap state density (about six times less than that of polycrystalline thin films) and high diffusion length (in the order of micrometers) (Minemoto *et al.*, 2015). An improvement on the efficiency of solar cells was recorded when single crystal or large grain sized perovskite material is used (Shi *et al.*, 2015). This remarkable improvement of the efficiency of perovskite is due to increased carrier mobility and diffusion length that arise because of reduction of charge trapping by narrowing the interfacial area that is associated with large grains that eliminate hysteresis, and the reduction in magnitude of bulk defects (Lian *et al.*, 2016) in the large grains. Therefore, highly crystalline perovskite material is needed for an improvement of solar cells. In spite of the drastic increase in the efficiency of PSCs, the issue of stability and environmental friendliness is still at stake. It has been unfolded that the organic molecules in the organo-inorganic hybrid perovskite have poor thermal and light stability (Minemoto *et al.*, 2015; Chen *et al.*, 2021). Frost and his co-worker recently researched into the causes of moisture instability of Organo-Inorganic Halid Perovskite (OIHP) and unfolded the possible cause of its instability in moist air. Bello *et al* (2021) highlighted the superiority of single crystal synthesis over polycrystalline counterpart. Their studies identified the absence of grain boundary in single crys-

*Corresponding author: ogabello2002@yahoo.com

¹Department of Mechanical Engineering, Ahmadu Bello University Zaria, Kaduna State

²Department of Mechanical Engineering, Bayero University, Kano

³Department of Chemical Engineering, Bayero University, Kano

⁴Advanced Membrane Technology Research Center, School of Chemical and Energy Engineering, Universiti Teknologi Malaysia, Malaysia, 81310 Johor, Johor Bahru

tal structure which account for its stability in adverse weather conditions.

During the last few years, a lot of research effort has been devoted to this end (Niu *et al.*, 2015; Leijtens *et al.*, 2017). The Structural stability of a material is an indication of its ability to sustain a certain crystalline phase to be stable at different condition of temperature, pressure and characterized by the absence of polymorphism (Leijtens *et al.*, 2017). The factors contributing to the poor stability of perovskites can be classified into two broad categories: extrinsic and intrinsic. Extrinsic factors are related to the environment such as oxygen and moisture, while the intrinsic factors include thermal instability, hygroscopicity and ion migration (Meng *et al.*, 2016). The inherent instability of the organo-inorganic halide perovskite solar cells on the exposure to moisture, air or oxygen, thermal and UV illumination contributes to the degradation of the perovskite absorber layer.

Frost *et al.* (2014) showed that MAPbI₃ would bind with a water molecule, and a proton in the methylamine ion would be captured, and finally leads to decomposing into a hydrate of methylamine and HI. It was inferred that replacing the organic ions of perovskite with proton-free ion groups, such as (CH₃)₄N⁺, would improve the stability of perovskite. Also, the presence of heavy metal in the most trending cluster (MAPbI₃) has deterred its commercialization in addition to its instability in moist air. Hence, this work explores the assertion of Frost and his co-worker to model a novel lead-free organo-inorganic halide perovskite and characterize it for environmentally friendliness and moisture stability and its potential application in photovoltaic cell.

Materials and Methods

The material used for the synthesis and fabrication are indium tin oxide (ITO)-coated glass (15 Ω.sq⁻¹), zinc powder of particle size 45 μm, hydrochloric (HCl) acid, scotch tape, de-ionized water, acetone, ultrasonic bath, titanium isopropoxide, isopropanol, Tetramethylammonium iodide ([CH₃]₄NI), barium iodide (BaI₂), agar mortal, glacial acetic acid, ultrasonic stirrer, filter paper, ethanol, and gamma-butyrolactone (GBL)

Perovskite cluster modelling of (CH₃)₄NBaI₃

The cluster (CH₃)₄NBaI₃ was formed in the format of perovskite structure such that A-site is occupied by (CH₃)₄N⁺, B-site is occupied by Ba and X-site is occupied by I. The structural stability of perovskites was estimated by the Goldschmidt Tolerance (GT) factor. The GT factor (t) of ABX₃ is expressed in Equation (1) as:

$$t' = \frac{R_{Aeff} + R_X}{\sqrt{2(R_B + R_X)}} \quad (1)$$

where R_{Aeff} is the effective ionic radius of organic cation, R_B is the ionic radius of divalent metal, R_X is the ionic radius of halide ion. The value of t for (CH₃)₄NBaI₃ was determined as 1.0198 given that $R_{Aeff} = 2.92\text{\AA}$, $R_B = 1.35\text{\AA}$ and $R_X = 2.20\text{\AA}$. The value of $t = 1.0198$ means the formation of (CH₃)₄NBaI₃ was possible and it was within the tolerance factor for organic halide perovskite. Using the extended tolerance formula given in the Equation (2),

$$t' = \frac{R_X}{R_B} - n_A \left(n_A - \frac{R_A/R_B}{\ln(R_A/R_B)} \right) \quad (2)$$

With $n_A = 1$, $t' = 3.43$ and less than 4.18. This indicated that the structure chosen was a perovskite. For stability of the structure, octahedra factor, which is defined as the ratio of the ionic radii

of the B cation and the halide anion, is given as Equation (3).

$$\mu = \frac{R_s}{R_x} \quad (3)$$

This indicated the stability of BX₆ octahedron, and it is limited within the range of $0.44 \leq \mu \leq 0.9$ for a stable perovskite. For (CH₃)₄NBaI₃, μ is equal to 0.6136, which is within the limit of stability of perovskite.

Synthesis of (CH₃)₄NBaI₃ crystals

All the reactants and the solvents were of analytical grade and used without further purification. The (CH₃)₄NBaI₃ crystals was synthesized as follows: 391 mg of BaI₂ (99.995 %, Sigma Aldrich) was measured in a conical flask. Excess (CH₃)₄NI of 210 mg (99 %, Sigma Aldrich) was measured and added and the mixture was grinded for 10 min in agar mortar. The resulting mixture was added gradually to 1 ml glacial acetic acid solution and simultaneously ultrasonically stirred at 500 rpm for 10 min in order to react completely. The solution was allowed to sediment and the precipitate was collected by filtration, and then washed repeatedly with ethanol in order to remove the residual (CH₃)₄NI. The product ((CH₃)₄NBaI₃) was finally dried at 60 °C in a vacuum overnight (Xianyu *et al.*, 2017).

Preparation of substrate

Indium doped tin oxide (ITO) coated glass sheet was cut to 15 x 20 mm (slot size of the depositing machine) using scissors and patterned using zinc powder and 2 M of HCl to etch it. The active area (unetched area) of ITO was covered with scotch tape leaving the area to be etched uncovered. The etched ITO was cleaned using ultrasonic bath with de-ionized water, acetone, and again de-ionized water at interval of 20 min and then dried with nitrogen flow to make the surface inert. Finally, the ITO was subjected to oxygen plasma treatment for 10 minutes to remove the remaining organic residues and make the surface hydrophilic.

Preparation of c-TiO₂

Compact TiO₂ was prepared in the following steps: 1.2ml of titanium isoprenoids was measured in a conical flask. 20 ml isopropanol was measured and added, followed by 4.4 ml HCl. The resulting solution was stirred ultrasonically at 1000 rpm for 10 s.

Perovskite solar cell fabrication

The device configuration of the fabricated solar cell is shown in Fig 2. The cleaned and patterned ITO was coated with a dense compact TiO₂ (c- TiO₂) layer. The compact layer was deposited unto the surface of the prepared ITO substrate using spin

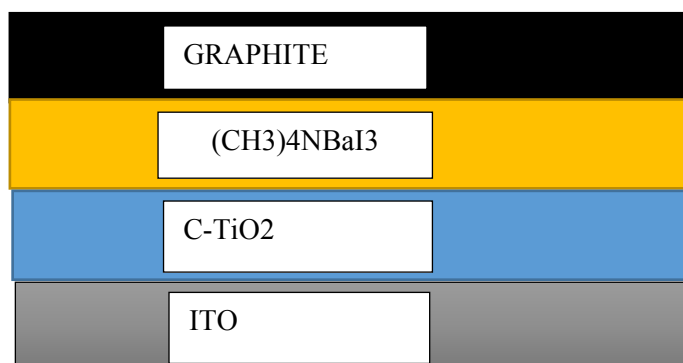


Figure 2 n-i-p planar perovskite structure: ITO, c-TiO₂, (CH₃)₄NBaI₃ and graphite anode

coater. c-TiO₂ layer was spin coated on the ITO substrate at 3000 rpm for 30 s. The etched portion of the ITO glass coated with c-TiO₂ was removed using cotton wool, and then rinsed in isopropanol to prevent c-TiO₂ from covering the whole substrate and then dried at 125 °C for 5 min on a hotplate and then sintered in a furnace at 450 °C for 30 min to form compact TiO₂ layer. The substrates were allowed to cool down to room temperature and then removed from the furnace.

A solution of 1M of (CH₃)₄NBaI₃ was mixed in 1 ml GBL and stirred for 4 h on a hot-plate. The resulting solution was spin-coated on the top of sintered c-TiO₂ layer using one-step deposition method and then treated with a multi-step slow annealing method. The substrate was left for 30 s after deposition to ensure an even wet film to form. The substrate was then transferred to a dark enclosure to prevent exposure to the atmosphere for graphite deposition. The sample was then transferred to thermal evaporator where graphite was thermally evaporated unto the perovskite substrate.

Characterization of the fabricated perovskite

To elucidate the phases present, the diffraction peaks in the produced (CH₃)₄NBaI₃, X-ray diffraction Rigaku Miniflex diffractometer) at an operating voltage of 40 kV and 30 mA current, and a scan between a 2θ range of 20–60 will be carried on the synthesized (CH₃)₄NBaI₃. The thermal stability of (CH₃)₄NBaI₃ crystal was examined through thermo-gravimetric analysis (TGA) using thermo-gravimetric analyzer and Differential Scanning Calorimetry (DSC) were used. A 11.6790 mg powder sample of as-produced (CH₃)₄NBaI₃ was placed in a sample pan located in furnace of thermo-gravimetric analyzer with a programmable temperature controller. The temperature was increased gradually at a constant rate of 5 °C/minute from 30 °C to 800 °C to incur a thermal reaction for 154 minutes and this was done under Nitrogen gas flow. The thermo-gravimetric data collected from a thermal reaction was compiled into a plot of mass against temperature and time (Juarez-Perez *et al.*, 2016). A sample of (CH₃)₄NBaI₃ was placed inside a crucible, which was then placed inside a DSC furnace alongside with a reference pan, which was emptied. The sample was heated isothermally at the rate of 10 °C/min with the temperature range of -50 °C – 250 °C. The heating and cooling thermograms were recorded for the prepared sample.

The air stability of the synthesized (CH₃)₄NBaI₃ crystal was studied by taking XRD of the crystal powder saved at atmospheric conditions in a snap cap vial just as produced and after one month (Pratheek and Predeep, 2020). The surface microstructure and morphologies of the samples was studied on a Hitachi FESEM model SU8020 equipment equipped with an electron dispersive spectrum (EDS) accessory. The photoluminescence spectra of perovskites were determined using photoluminescence spectrometer. (CH₃)₄NBaI₃ was deposited on quartz disc using spin coater. After the deposition of (CH₃)₄NBaI₃ layer, the film was annealed on a hotplate at 100 °C. Photoluminescence emission spectra and absorption spectra was measured using FLS1000 photoluminescence spectrometer. The perovskite coated quartz discs was positioned using the face sample holder. The UV-visible measurements were performed using UV3600plus series version 2.52. The powdered sample was scanned with medium speed in the wavelength rang of 300 nm to 850 nm.

The electrical properties to be measured are fill factor, open circuit voltage (V_{oc}) and short circuit current (I_{sc}). The J–V characteristics of the perovskite solar cells, which will include the forward and reverse scans (–10 to 10 V, 200 mV s⁻¹) and steady-state power output were measured using Ossila solar cell I–V testing system 1.5 solar simulator (100 mW cm⁻²). All

tests were performed under ambient condition (Hache and Meier, 2002).

Results and Discussion

The structure and the elemental composition of the synthesized tetramethylammonium barium iodide perovskite was studied using the X-ray diffraction technique as illustrated in Figure 3.

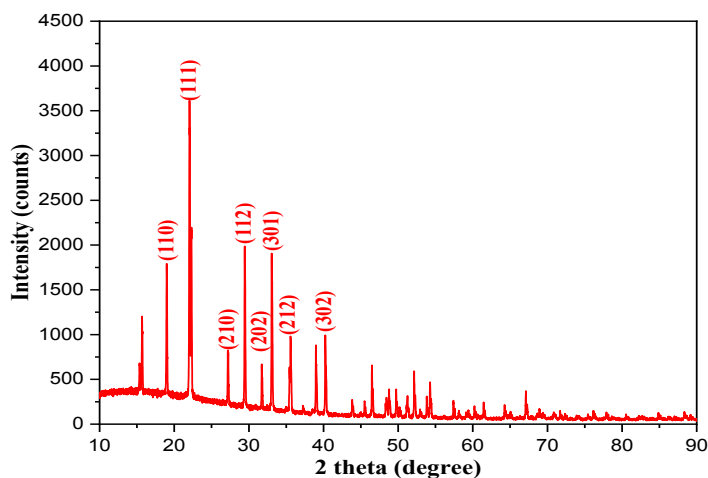


Figure 3 The XRD pattern of the synthesized tetramethylammonium barium iodide perovskite

The XRD pattern shown in Figure 3 was used to authenticate the structural formation of the synthesized (CH₃)₄NI. It was observed that the prominent peak of tetramethylammonium barium iodide reflection was at 2θ = 22.1° and other peaks were at around 19.0°, 29.5° and 33.3°. The XRD peaks are strong and the half peak width is narrow. These indicate that the perovskite (CH₃)₄NBaI₃ crystal has good crystallinity (Zhou *et al.*, 2017). The crystalline feature with narrow and sharp peaks of the synthesized (CH₃)₄NBaI₃ might imply high crystallinity and low average crystallite size. The high peaks might indicate the effective substitution of the I ion by the Ba ion in the perovskite lattice (Dads *et al.*, 2016).

The stability of the perovskite film in a moist environment was examined using the XRD technique. Fig 4 shows the comparison of the XRD pattern of the (CH₃)₄NBaI₃ Sample B as-prepared while sample B (4wks) was the sample exposed to the moisture environment for 4 weeks. It further shows the relative intensities of the various peaks so as to give a clearer picture of the change in peak due to degradation.

The XRD profile of the as-synthesized and after four

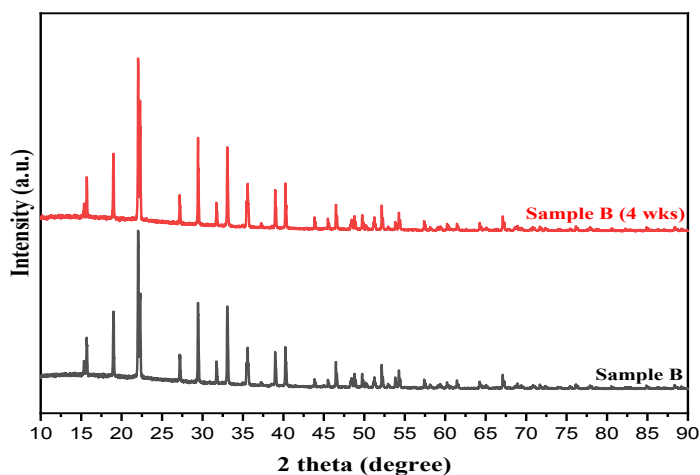


Figure 4 The XRD spectra of the as-prepared sample and when exposed to a moist environment

weeks samples are shown in Fig 5. XRD technique is used to evaluate the crystallinity and the average crystallite size. As it can be seen from the diffractograms, the material still retained all its structural characteristics. Hence, no peak shift or structure distortion was observed in the peaks, which depleted that there was no internal stress and the $(\text{CH}_3)_4\text{N}\text{BaI}_3$ sample was said to be stable. The average crystallite size was estimated from the full width of Half Maximum (FWHM) of the peaks using Scherrer's equation as stated in Equation 4.

$$D_A = \frac{K\lambda}{L\cos\theta} \quad (4)$$

Where D_A is the average crystallite size, K = dimensionless shape factor (0.9), λ = X-ray wavelength, L = FWHM and θ = Bragg angle. The average crystallite size for the as-prepared sample was 43 nm while the sample after exposure to the moisture environment was 39 nm. The reduction in the crystallite size attributed to water adsorption on the surface of the crystals. The average crystallinity of the sample was 90 %.

The surface morphology and elemental constituents of the tetramethylammonium Barium iodide was evaluated using a field emission scanning electron microscope (FESEM) with an energy dispersive X-ray analyzer (EDS) as presented in Fig 5.

The FESEM result as seen in Fig. 6 shows a plate-like structure composed of hexagonal crystal shapes and agglomerated in nature. As seen in the micrograph, the sample consists of fine and coarse grains, which might improve the photo-excited electrons diffusion through aggregating the light scattering properties and effective mean path of light of the perovskite (Tafazoli *et al.*, 2018). The EDS spectrum reveals the presence of I, C, N and Ba elements; the percentage composition of as-synthesized and the theoretical percentage composition are shown in Table 1. The remaining 8.9 % gives the percentage of Hydrogen EDS software does not include in its database. The variation in the percentage composition of the as-synthesized and the theoretical values is due to mass action law or chemical equilibrium of

the limiting reagents that are in excess of the reaction (Chung, 2020). The average particle size from FESEM is 23 μm . The thermogravimetric analysis of the tetramethylammonium barium iodide perovskite is illustrated in Fig 6.

Table 1 Percentage composition of the synthesized perovskite

No	Element	% Composition of As-synthesized	% Theoretical Composition
1	Iodine (I)	51.1	56.58
2	Carbon (C)	38.2	17.08
3	Nitrogen (N)	0.2	4.98
4	Barium (Ba)	1.6	19.93
5	Hydrogen (H)	8.9	4.27

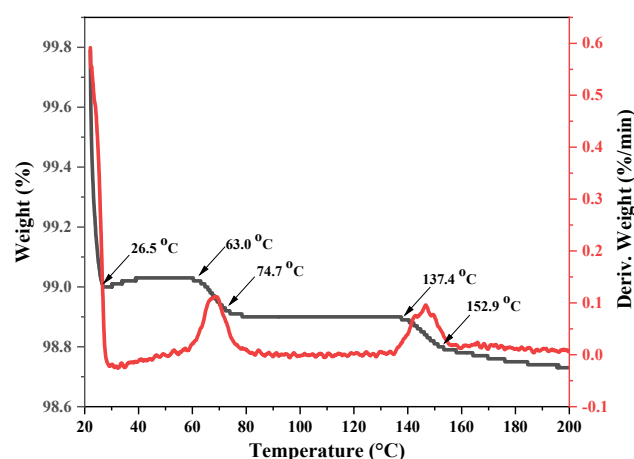


Figure 6 Thermogravimetric analysis and derivative weight of the tetramethylammonium barium iodide perovskite

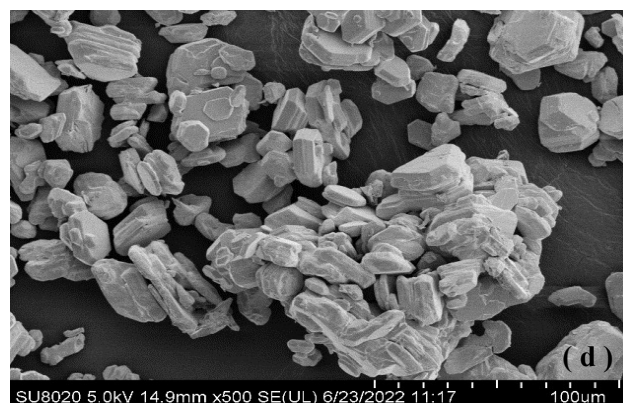
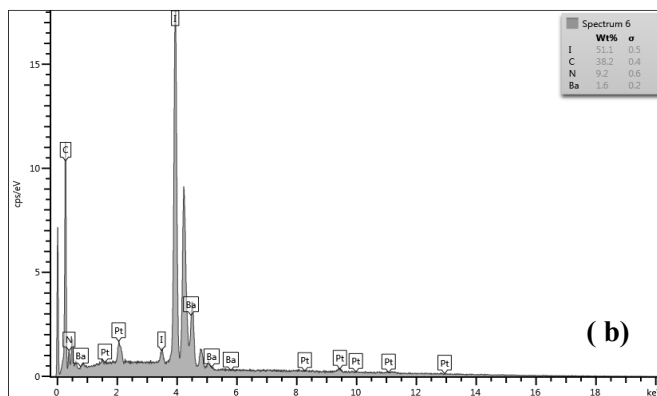
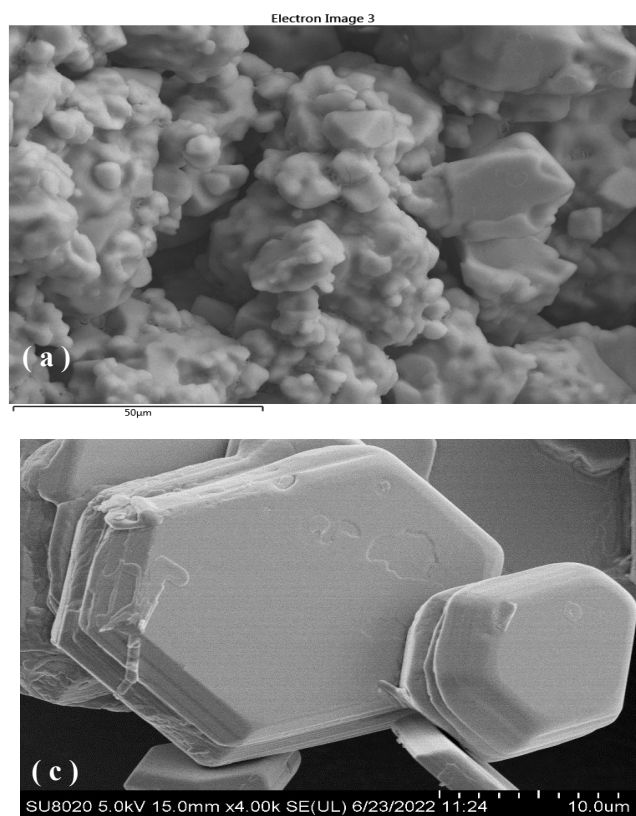


Figure 5 FESEM/EDS image of tetramethylammonium barium iodide (a) crystal on a scale of 50 μm , (b) EDS thermograph, (c) Crystal on a scale of 100 μm and (d) Crystal on a scale of 10 μm

The $(\text{CH}_3)_4\text{NBaI}_3$ exhibits two distinct weight loss steps at 22 – 26.5 °C and 63 – 200 °C. The initial weight loss was 0.8 % (0.093 mg) and corresponds to a total mass of 11.6790 mg of $(\text{CH}_3)_4\text{NBaI}_3$. The second step showed a weight loss of 1 % (0.117 mg) of the total mass. The result showed that the organic substituted Ba is stable which might be attributed to the higher volatility and hydrophilic feature of Ba (Xu *et al.*, 2016). In addition, this shows that the amine group is bounded into the $(\text{CH}_3)_4\text{NBaI}_3$ perovskite sample. As seen in the thermograph, the $(\text{CH}_3)_4\text{NBaI}_3$ perovskite sample seems to be stable at high temperatures with little change up to 200 °C and this suggests clear sublimation without complex decomposition (Baikie *et al.*, 2013). The organic components $(\text{CH}_3)_4\text{N}$ seem to be more stabilized in the tetramethylammonium barium iodide perovskite structure since very minimal weight loss was observed at the sublimation temperature coupled with little thermal decomposition (Liu *et al.*, 2015 and Zhou *et al.*, 2017). The differential scanning calorimetry (DSC) result of the Tetramethylammonium barium iodide synthesized is presented in Fig 7.

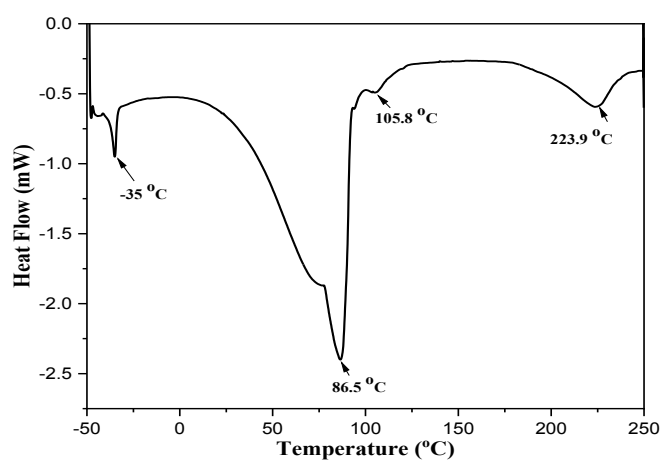


Figure 7 Differential scanning calorimetry for the synthesized tetramethylammonium barium iodide

From the DSC pattern as shown in Fig. 7, a broad peak attributed to an endothermic peak was observed between 30 and 99 °C but peaked near 86.5 °C is as a result of water that got trapped during crystal formation (Pratheek and Preddep., 2020). The removal of the OH group from water vaporization of water that got trapped during crystallization process (Baikie *et al.*, 2013). After the endothermic stage, the peak seems to disappear which might possibly be the reason for the stability of synthesized $(\text{CH}_3)_4\text{NBaI}_3$ sample observed in the thermo-

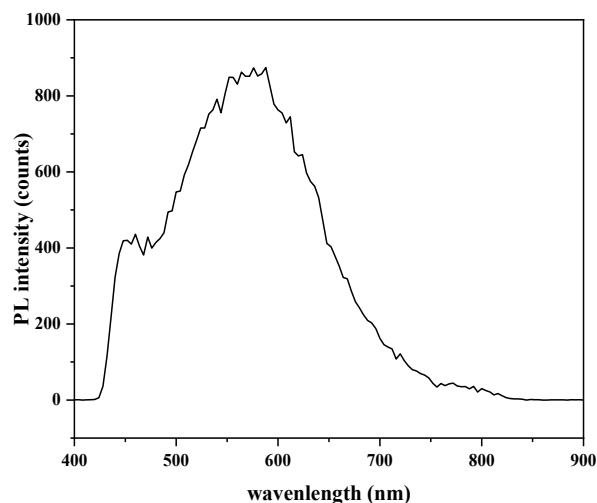


Figure 8 Steady-state photoluminescence decay of tetramethylammonium barium iodide

gram (Pratheek and Preddep, 2020). The transition at -35 °C showed small hysteresis whereas the others showed large hysteresis. Another endothermic peak was seen between 200 and 240 °C with the peak at 223.9 °C which shows gradual decomposition of the perovskite material (Kaltzoglou *et al.*, 2017).

Based on the DSC curve, the perovskite could be said to be thermally stable up to 200 °C. The photoluminescence spectrum of the tetramethylammonium barium iodide is presented in Figure 8. The emission spectrum of the synthesized $(\text{CH}_3)_4\text{NBaI}_3$ as presented in Fig 8 exhibits broad emissions within the range of 540 and 588 nm. The spectrum is similar to the one reported by Fu *et al.* (2016) except for the peaks at 459 and 497 nm which might be attributed to the presence of Barium in the sample. The Ultraviolet-visible absorption spectrum of the synthesized tetramethylammonium barium iodide as illustrated in Figure 9.

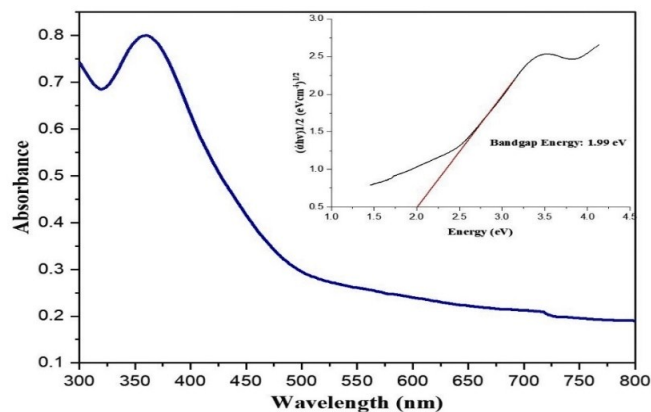


Figure 9 The absorbance and the energy band of $(\text{CH}_3)_4\text{NBaI}_3$

The Ultraviolet-visible absorption spectrum of the synthesized tetramethylammonium barium iodide as illustrated in Fig 9 gives a one hump feature as a result of the specifics of the band structure. The spectrum exhibits a strong optical absorption peak of wide bandgap semiconducting oxide and an intense absorption band around 360 nm. The powder exhibits a strong absorption in the visible range which extends from 360 nm to 725 nm. The absorption spectrum revealed that the $(\text{CH}_3)_4\text{NBaI}_3$ perovskite covers the broad spectrum indicating that its selection in photosensitive applications is appropriate (Tahseen *et al.*, 2019) and also tends to be transparent in the visible range of light from 725 nm to 850 nm, which is suitable for photovoltaic application. Additionally, the graph shows that absorption starts from around 500 nm. From the UV-vis curve, the estimated band gap energy of $(\text{CH}_3)_4\text{NBaI}_3$ is 1.99eV. From the spectrum, it can be deduced that the $(\text{CH}_3)_4\text{NBaI}_3$ nanoparticles respond to the ultraviolet adequately.

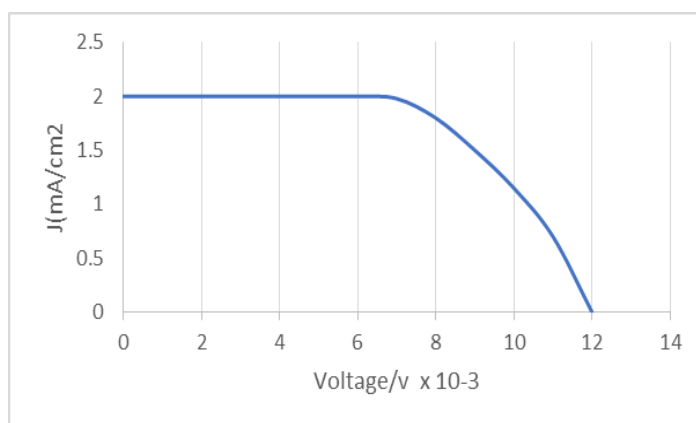


Figure 10 The J-V curve of the synthesized $(\text{CH}_3)_4\text{BaI}_3$

Table 2 Photovoltaic parameters of (CH₃)₄BaI₃/graphite based perovskite with forward and reverse scanning

Scan Pixel Area	Mode of Scanning	PCE (%)	FF (%)	J _{sc} (mA.cm ²)	V _{oc} (V)	MP (W)	R _{series} (Ohm.cm ²)	R _{shunt} (Ohm.cm ²)
0.04cm ²	Forward Scan	4.5	19.37	1.906	0.012	4.5	6.1	6.1
	Reversed Scan	4.6	19.56	2	0.012	4.6	6	6

The J-V characterization of the solar cell was measured using Ossila solar cell I-V testing system within the scan voltage of -1.0 to 1.2V for both forward and reversed scan with voltage increment of 0.3503V. The pixels scanned area of 0.04cm² were used for the scanning. The measured parameters are shown in Table 2. The J-V characterization of the synthesized (CH₃)₄BaI₃ was presented in Fig 10 with current density of 2mA/cm² and Voc of 12 x 10⁻³mA.

Conclusion

The main objective of this research work, which was to model, synthesis and characterize environmentally stable novel lead-free organo-inorganic halide perovskite, was achieved. Based on the achievements of this research work, the following inferences have been drawn. The stability of the novel perovskites was attributed to two factors that were considered; firstly, the modelled cluster successfully met the three generalized Goldschmidt factors as stated in the methodology. Secondly, the use of proton free organic mono-cation, (CH₃)₄N⁺, does not give room to air (oxygen) to act on the synthesized perovskite, thereby responsible for its moisture stability test.

The synthesized novel perovskite was thermally stable for solar cell application as it requires very high temperature (> 200 °C) for its degradation to be noticed. However, a PCE of 4.6 % was achieved. It is therefore recommended that more research work should be done on its synthesis and moisture stability test to ascertain the stability of the perovskite cluster since it is a novel perovskite cluster.

Conflict of Interest Declarations

The authors declare no conflict of interest.

References

- Bello, A., Alhaji, A., Mokoyo, M., Nurudeen, S., Aziz, F., (2021). A review of the pathways to the synthesis of single crystal perovskite cluster. *The Nigerian Journal of Tropical Engineering*, 14 (1), pp 346-358.
- Chung, D., Linker, C., Chi, W., (2020). All-inorganic perovskite CsPbX₃ electrospun nanofibers with color-tunable photoluminescence and high-performance optoelectronic applications. *Journal of Alloys and Compounds*, 830(1), pp 432-446. <https://doi.org/10.1016/j.jallcom.2020.157426>
- Dads A., Bouzit, S., Nkhaili, L., Elkissani, A., and Outzourhit, A. (2016). Structural, optical and electrical properties of planar mixed perovskite halides/Al-doped Zinc oxide solar cells. *Solar Energy Materials and Solar Cells*, 148 (1), pp. 30-33.
- Ding C., Yaohong Z., Feng L., Yukiko K., Shuzi H., Taro, T., Kenji Y., Takashi M., Kenji K., Qing S, (2018). Effect of the conduction band offset on interfacial recombination behavior of the planar perovskite solar cells. *Nano Energy*, 53 (1), pp. 17-26.
- Dong, Q., Y., Fang, Y., Shao, Y., (2015). Solar cells. Electron-hole diffusion lengths > 175 μm in solution-grown CH₃NH₃PbI₃ single crystals. *Science Journal*, 347 (6225), pp. 967-70. <https://doi.org/10.1126/science.aaa5760>.
- Frost, J., M., Butler, K., T., Brivio, F., Hendon, C., H., van Schilfgaarde, M., Walsh A (2014). Atomistic origins of high-performance in hybrid halide perovskite solar cells, *Nano Letters*, 14, pp. 2584–2590.
- Hacke, P.; Meier, D., L., (2002). Analysis of fill factor losses using current-voltage curves obtained under dark and illuminated conditions. *Proceedings of 29th IEEE Photovoltaic Specialists Conference*, pp. 462-464.
- Juarez, E., J., Hawash, Z., Raga, S., R., Ono, L., K., & Qi, Y., (2016). Thermal degradation of CH₃NH₃PbI₃ perovskite into NH₃ and CH₃I gases observed by coupled thermogravimetry–mass spectrometry analysis. *Energy & Environmental Science*, 9(11), 3406–3410. <https://doi.org/10.1039/c6ee02016>.
- Kaltzoglou, A., Stoumpos, C., C., Kontos, A., G., Manolis, G., K., Papadopoulos, K., Papadokostaki, K., G., and Falaras, P. (2017). Trimethylsulfonium lead triiodide: an air-stable hybrid halide perovskite. *Inorganic Chemistry*, 56(11), 6302-6309.
- Lian Z., Q., Yan, T., Gao, J., Ding, Q., Lv, C., Ning, Q., Li, J.L. Sun (2016). Perovskite CH₃NH₃PbI₃(Cl) single crystals: rapid solution growth, unparalleled crystalline quality, and low trap density toward 108 cm⁻³. *Journal of the American Chemical Society*, 138, pp. 9409–9412. <https://doi.org/10.1021/jacs.6b05683>.
- Leijtens, T., Bush, K., Cheacharoen, R., Beal, R., Bowring, A., McGehee, M.D., (2017). Towards enabling stable lead halide perovskite solar cells; interplay between structural, environmental, and thermal stability. *Journal of Material Chemistry*, A5, pp. 11483–11500.
- Liu, Y., Yang, Z., Cui, D., Ren, X., Sun, J., Liu, X., ... & Liu, S., (2015). Two-inch-sized perovskite CH₃NH₃PbX₃ (X= Cl, Br, I) crystals: growth and characterization. *Advanced Materials*, 27(35), pp. 5176-5183.
- Meng L, J., You, T.-F. Guo, Y. Yang, (2016). Recent advances in the inverted planar structure of perovskite solar cells. *Accounts of Chemical Research*, 49(1), pp. 155–165.
- Minemoto, T., Masashi, M., (2015). Theoretical analysis on effect of band offsets in perovskite solar cells *Solar Energy Materials and Solar Cells*, 113, pp. 8-14. <https://doi.org/10.1016/j.solmat.2014.10.036>.
- Niu, G., Guo, X., Wang, L., (2015). Review of recent progress in chemical stability of perovskite solar cells. *Journal of Material Chemistry*, A3, pp. 8970–8980.
- Pratheek, M, P., Predeep (2020). Hybrid perovskite single crystal with extended absorption edge and environmental stability: Towards a simple and easy synthesis procedure. *Materials Chemistry and Physics*, 239(1), 122084.
- Stranks S., D., Eperon, G., E., G., Grancini, C., Menelaou, M., J., P., Alcocer, T. Leijtens, L. M. Herz, A. Petrozza, H., J., Snaith, (2013). Electron-hole diffusion lengths exceeding 1 micrometer in an organometal trihalide perovskite absorber. *Science*, 342, pp. 341–344. <https://doi.org/10.1126/science.1243982>.
- Shi, D., Adinolfi, V., Comin, R., Yuan, M., et al. (2015). Low trap-state density and long carrier diffusion in organolead

- trihalide perovskite single crystals. *Science*, 347, pp. 519–522. <https://doi.org/10.1126/science.aaa2725>.
- Tafazoli, S., Timasi, N., Nouri, E., & Mohammadi, M. R. (2018). The role of a vapor-assisted solution process on tailoring the chemical composition and morphology of mixed-halide perovskite solar cells. *CrystEngComm*, 20 (31), pp. 4428-4435.
- Tvingstedt, K., Gil-Escrig, L., Momblona, C., Rieder, P., Kiermasch, D., Sessolo, M., Baumann, A., Bolink, H.J., Dyakonov, V., (2017). Removing leakage and surface recombination in planar perovskite solar cells. *ACS Energy Letters*, 2(2), pp. 424-430.
- Warner T., E., (2012). Synthesis, properties and mineralogy of important inorganic materials. John Wiley & Sons, pp 146-148. <https://doi.org/10.1002/9780470976012>.
- Xianyu, J., Ziyang, H., Yubin, Z., (2017). Facile synthesis of organic–inorganic hybrid perovskite $\text{CH}_3\text{NH}_3\text{PbI}_3$ microcrystals. *Journal of Alloys and Compounds*, 725 <https://doi.org/10.1016/j.jallcom.2017.07.154>
- Xing G., N., Mathews, S., Sun, S.S. Lim, Y.M. Lam, M. Graetzel, S., Mhaisalkar, T., C., Sum, (2013). Long-range balanced electron-and hole-transport lengths in organic inorganic $\text{CH}_3\text{NH}_3\text{PbI}_3$. *Science*, 342, pp. 344–347. <https://doi.org/10.1126/science.1243167>.
- Zhou, J., Xia, Z., Molokeev, M., S., Zhang, X., Peng, D., and Liu, Q., (2017). Composition design, optical gap and stability investigations of lead-free halide double perovskite $\text{Cs}_2\text{AgInCl}_6$. *Journal of Materials Chemistry*, A5(29), pp. 15031-15037.